Journal of Physics:
Conference Series

PAPER • **OPEN ACCESS**

Three-dimensional simulation of a floating wind turbine platform

To cite this article: Giovanni Caramia *et al* 2024 *J. Phys.: Conf. Ser.* **2893** 012019

Journal of Physics: Conference Series **2893** (2024) 012019 doi:10.1088/1742-6596/2893/1/012019

Three-dimensional simulation of a floating wind turbine platform

Giovanni Caramia[1], Andrea Fiore[1], Marco Genualdo[1], Pietro De Palma[1] and Riccardo Amirante[1]

[1]Dipartimento di Meccanica Matematica e Management, Politechnic University of Bari, Bari, Italy

E-mail: giovanni.caramia@poliba.it

Abstract. As the need for renewable energy has grown in recent years, the possibility of creating and collecting deep-sea wind energy has become a research hotspot. Floating wind turbines need platforms to provide a stable working state and structural safety. This article focuses on the study of the dynamics of the deep-water semi-submersible floating platform OC4-DeepCwind. The open-source computational fluid dynamic toolbox OpenFOAM is used for comparative analysis of the floating structure motion response. In order to eliminate the influence of grid size and refinement level on the simulation results, a grid refinement study was conducted before detailed hydrodynamic discussions. In absence of wind, the dynamic response of the platform is studied under the influence of the impact with regular waves with different amplitudes. The effect of the presence of the tower supporting the wind turbine on the dynamics of the platform is investigated as well. Results show that the addition of the tower exerted a slight destabilising influence on the support's dynamic behaviour, confirming its stability against different wave height. Finally, the model has demonstrated its efficacy as a highly valuable tool for the simulation of wind turbines on floating foundations.

1 Introduction

The growing awareness of climate change and its effects has highlighted the urgent need to reduce greenhouse gas emissions. Renewable energy sources, such as wind power, represent a sustainable solution to address these challenges. They provide a pathway towards a cleaner and robust energy conversion system satisfying the energy demand and reducing the environmental carbon footprint in a future scenario. Offshore wind energy represents one of the most promising non-polluting frontiers in the field of renewable energy [1], [2], [3], [4], [5]. This is evidenced by the significant interest it is generating not only in the academic world among universities and researchers, but also among governments [6]. A report published by the European Wind Energy Association (EWEA) [7] indicates that the European Commission anticipates the installation of 305 GW of cumulative wind energy capacity by 2030, representing a significant increase of 176 GW over that of the end of 2014. Concurrent with the growth of the offshore wind industry, a new generation of floating offshore wind turbines (FOWTs) is being developed [8]. Several floating wind farms have been developed, with the first full-scale 2.3-MW floating wind turbine being installed at Hywind, near the coast of Norway. Additionally, five 6-MW floating wind turbines were installed in the North Sea, off the coast of Peterhead (Scotland). Furthermore, Kincardine (50 MW, Scotland) and Windfloat Atlantic (25 MW, Portugal) farms have also been installed. Indeed, Rapella et al. [9] confirm that Europe is playing a key

role in the renewable energy transition and will be a pioneer in the offshore field with the British Islands, North Sea, Balkan Peninsula, as well as the areas of the south of France, Central Mediterranean and north of Spain, standing out as particularly promising regions. In Central Mediterranean and Balkan Peninsula, the number of low wind events has increased, yet climate change is not expected to have a significant impact on the average near-surface wind speed [10], nor on the average energy production [9].
The primary motivation behind the growing interest in FOWTs is the substantial advantage associated with offshore wind energy. One of the most significant benefits is the availability of stronger and more consistent winds on the sea compared to on-shore locations, which leads to higher and more reliable energy production. The expansive ocean areas allow for the installation of larger turbines and extensive wind farms, significantly increasing the overall energy output. Additionally, offshore wind farms have minimal visual pollution and noise impact on local communities due to their distance from residential areas. As stated by Vorpahl et al. [11], offshore wind turbines are "low risk structures" for these reasons.
Nevertheless, the development of offshore wind energy is not without challenges. Rapella et al. [9] have highlighted that wind energy is one of the most variable and weather-dependent renewable energy sources, as it relies on wind speed, which is influenced by daily to seasonal variations. Numerical analysis is one of many key tools during the initial FOWT design stage [12], which aims to predicting the turbine work under real environmental and wind conditions. The design of FOWT systems is a challenging endeavour due to the complicated structure, the intricate environmental loading, and the coupling effects [13], [5]. Furthermore, the significant increase of commercial wind turbine dimensions, driven by economy of scale, and the interplay between blade and tower systems, introduces several uncertainties regarding the forecasting of aerodynamic loads and wake dynamics [13].
Consequently, it is really challenging to operate a full-scale test model on this technology due to the influence of multiple physical phenomena and the dependence on extreme weather conditions with a cut-out speed of approximately 25 m/s [14].
To fulfil the need for forecasting the combined aerodynamic and hydrodynamic behaviours of a FOWT system, numerical methods stand out as the most appropriate approach. This is due to their cost-effectiveness compared to experimental tests and their independence from scaling laws. Otter et al. [15] provided an overview of high, mid and low fidelity software modelling offshore wind turbines. They divided computational tools into three categories based on their purpose: structural, hydrodynamic and aerodynamic. OpenFOAM, a CFD computational development framework, is regarded as a high-fidelity modelling tool for offshore wind turbines. OpenFOAM is employed for simulations across the entire marine field, including WECs (Wave Energy Converters) [16], and is particularly suited to modelling FOWTs, as evidenced by numerous studies.
The present study focuses on the OC4-DeepCwind semisubmersible floating wind system, in conjunction with the NREL 5-MW baseline wind turbine developed by the National Renewable Energy Laboratory (NREL), as an illustrative example of the proposed numerical framework for estimating the offshore wind turbine behaviour. The system under consideration has six Degree of Freedom (6-DOF) subjected to waves with a fixed period (T) and height (H), which are analysed using OpenFOAM.
The three-dimensional unsteady Reynolds-averaged Navier–Stokes (URANS) equations coupled with the $k-\omega$ SST turbulence model are solved. The PIMPLE algorithm is employed to solve the pressure-velocity coupling equations.

2 Method

In the OpenFOAM development framework, overInterDyMFoam is a solver designed for transient simulations of two incompressible, isothermal, and immiscible fluids. It is capable of handling both laminar and turbulent flows of Newtonian and non-Newtonian fluids. The solver employs the volume-of-fluid (VOF) method to accurately capture the interface between the fluids.
Based on interFoam, the solver enhances its predecessor's capabilities by incorporating overset (Chimera) meshes. This advancement makes the solver particularly suitable for scenarios involving significant motion of objects, where traditional dynamic meshes prove inadequate.
The overset framework offers a universal approach to implementing overlapping meshes for both stationary and dynamic scenarios. It utilizes mappings from cell to cell across various, separate mesh regions to create a unified domain. This approach facilitates intricate mesh movements and interactions without the drawbacks typical of mesh deformation, including both single-phase and multi-phase flow modelling.
The solver uses the PIMPLE (merged PISO-SIMPLE) algorithm for pressure-momentum coupling. This algorithm leverages the strengths of both PISO and SIMPLE methods for pressure-velocity coupling,

ensuring robustness in handling transient flows with large time steps. This approach is supplemented by under-relaxation techniques to secure convergence stability. It supports Multiple Reference Frame approach and porosity modelling and allows easy integration of passive scalar transport equations and source terms. Furthermore, the solver itself handles mesh movements and deformations.
The applications of the solver are akin to those of interFoam, but with the added functionality of overset meshes. It can simulate very large object motions. This is particularly useful in the marine industry for simulating the movement of floating objects or hulls in presence of high waves. It also allows one to model ship rotors, taking their motion into account during simulations.

2.1 interFoam

OpenFOAM® (interFoam solver) solves the URANS equations for two-phase incompressible flows using the VOF technique. The pressure and velocity fields are obtained solving the continuity (Eq. 1) and momentum conservation (Eq. 2) equations. The free surface is tracked by Eq. 3

$$\nabla \cdot \mathbf{U} = 0, \tag{1}$$

$$\begin{aligned} \frac{\partial \rho \mathbf{U}}{\partial t} + \nabla \cdot (\rho \mathbf{U}\mathbf{U}) - \nabla \cdot (\mu_{eff} \nabla \mathbf{U}) = \\ -\nabla p^* - \mathbf{g} \cdot \mathbf{X} \nabla \rho + \nabla \mathbf{U} \cdot \nabla \mu_{eff} + \sigma \kappa \nabla \alpha_1, \end{aligned} \tag{2}$$

$$\frac{\partial \alpha_1}{\partial t} + \nabla \cdot \mathbf{U}\alpha_1 + \nabla \cdot \mathbf{U}_c \alpha_1 (1 - \alpha_1) = 0. \tag{3}$$

In these equations $\mathbf{U}$ is the velocity vector; $\mu_{eff} = \mu + \mu_{turb}$ is the effective dynamic viscosity; p^* is defined as $p^* = p - \rho \mathbf{g} \mathbf{X}$, being p the static pressure; $\mathbf{X}$ is the position vector; α is the volume fraction of phase 1. The last term in Eq. 2 accounts for surface tension effects: σ is the surface tension coefficient; $\kappa = 1/4 \nabla \cdot (\nabla \alpha_1 / |\nabla \alpha_1|)$ is the curvature of the interface. The last term in Eq. 3 is a numerical source term to avoid the excessive diffusion of the interface, being $\mathbf{U}_c$ the compression velocity. Since pressure and velocity are coupled, the solution of both fields is obtained with a two step approach. The URANS equations are discetized by a standard finite volume approach using the OpenFOAM® library, which employs the PIMPLE method originated by merging PISO and SIMPLE algorithms. The solution of Eq. 3 has to be bounded between 0 and 1. OpenFOAM®'s special approach called MULES (Multidimensional Universal Limiter for Explicit Solution) uses a limiter function on the numerical fluxes to fulfil these restrictions. For further reference regarding the governing equations and the discretization procedure, see references [17] and [18].

2.2 Rigid body motion solver

The native rigid body motion solver in OpenFOAM®, i.e. sixDoFRigidBodyMotion, is applied to solve the six degrees of freedom motion of the floating body. The dynamics of the body motion is governed by the linear and angular momentum conservation laws:

$$\mathbf{a}_f = \mathbf{F}_f / m_f, \tag{4}$$

$$\theta_f = \mathbf{I}_f^{-1} \cdot \mathbf{M}_f, \tag{5}$$

where $\mathbf{a}_f$ and θ_f are the linear and angular acceleration vectors of the floating body, respectively; m_f and $\mathbf{I}_f$ are the mass and moment of inertia of the floating body. External force and moment, $\mathbf{F}_f$ and $\mathbf{M}_f$, are calculated as:

$$\mathbf{F}_f = \iint_S (p\mathbf{I} + \tau) \cdot d\mathbf{S} + m_f \mathbf{g}, \tag{6}$$

$$\mathbf{M}_f = \iint_S \mathbf{r}_{CS} \times (p\mathbf{I} + \tau) \cdot d\mathbf{S} + \mathbf{r}_{CG} \times m_f \mathbf{g}, \tag{7}$$

where $\mathbf{I}$ is the identity matrix, τ is the viscous stress tensor and $\mathbf{S}$ is the surface of the boundary patch of the floating body. $\mathbf{r}_{CS}$ and $\mathbf{r}_{CG}$ are the hydrodynamic and gravity forces, respectively. Based on the linear and angular acceleration computed by Eq. 4 and Eq. 5, the Newmark [19] integration scheme is employed to obtain the velocity and position vectors, namely,

$$\mathbf{u}_{f,n}^{k+1} = \mathbf{u}_{f,o} + \Delta t \left(\gamma \mathbf{a}_{f,n}^{k} + (1 - \gamma) \mathbf{a}_{f,o} \right), \tag{8}$$

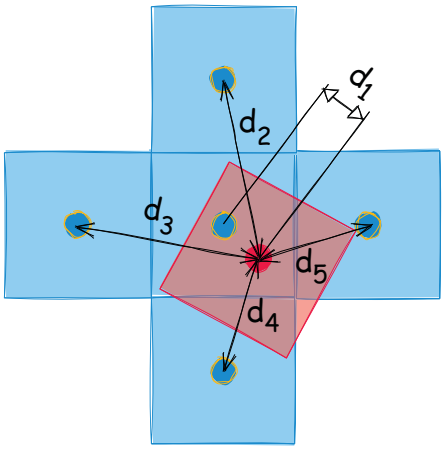

(a) Diagram of overlapping meshes: the arrows indicate the distance between cell centres, the red cell is receptor and the blue ones are donors.

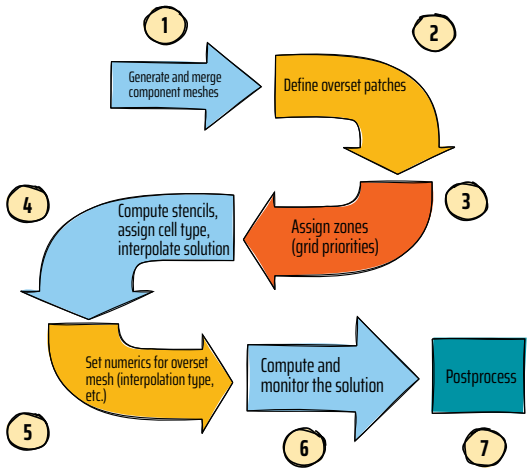

(b) Overset simulation workflow.

Figure 1: Overset mesh (left), overset workflow (right).

$$\mathbf{x}_{f,n}^{k+1} = \mathbf{x}_{f,o} + \mathbf{u}_{f,o}\Delta t + \beta(\Delta t)^2\mathbf{a}_{f,n}^{k} + (0.5-\beta)(\Delta t)^2\mathbf{a}_{f,o}, \tag{9}$$

where Δt is the time step, γ and β are two parameters of the Newmark scheme. In the present work, the commonly used parameters values $\gamma = 0.5$ and $\beta = 0.25$ are adopted, yielding the so-called constant average acceleration method. The second subscript for $\mathbf{u}_f$ and $\mathbf{x}_f$ indicates the value at either the old time step (i.e. $\mathbf{u}_{f,o}$) or the new time step (i.e. $\mathbf{a}_{f,n}$). This scheme allows implicit sub-iterations within one time step, so the superscript k indicates $k-th$ sub-iteration.

2.3 Overset mesh

The advantage of the overset mesh method is that it allows one to use several overlapping meshes to deal with complex geometries. Each mesh block can handle a part of the domain with the possibility to move following or not a prescribed law. A simple example of two overlapping meshes is shown in figure 1a. A background grid is firstly generated to discretise the whole domain without considering the body geometry. Then a body-fitted grid conforming to a given geometry is generated and overlapped to the background mesh. For complex problems, multiple component meshes can be generated and introduced in the domain. Before solving the flow equations, all the component meshes need to be assembled to determine the domain connectivity information. This includes three key steps:

1. *Hole cutting*: Points and cells inside (and close to) the body surface, usually called *hole points/cells*, are identified and deactivated. A common practice is to mark hole points/cells with a tag to exclude them from the flow calculation.

2. *Fringe search*: The points/cells surrounding the hole, usually named *fringe points/cells*, are selected and used to exchange information between component meshes.

3. *Donor search*: For each fringe point/cell, one or several points/cells from a component mesh need to be selected as the donor(s) to send the information to the receptor. Figure 1a shows a receptor point (red) on the fringe region and its donor points (blue) on the background mesh.

Figure 1b shows the overset mesh simulation workflow in OpenFOAM®. This solver uses a distance based implicit method aided by a regular voxel mesh to quickly cut out the hole from all the component meshes. A detailed description of this hole cutting method is provided by [20] and [21]. For fixed boundary problems, the assembly algorithm needs to be executed only once before the flow calculation. For deforming and/or moving boundaries, the assembly needs to be executed every time step.
As we have seen, the exchange of information between component meshes is accomplished through the use of receptor and donor cells in the fringe region. The flow variables ϕ_r at the receptor are obtained

Quantity	Measure
Height	77.6 m
External diameter	6.5 m
Internal diameter	6.462 m
Density	8500 kg/m^3

Table 1: Tower geometry and material.

through an interpolation of the donor values. Linear, bi-linear, least square or other interpolation methods can be used to exchange of information between component meshes. In the present work, we used a distance weighted function

$$\phi_r = \frac{\sum_{i=1}^{N} \phi_i/d_i}{\sum_{i=1}^{N} 1/d_i}, \tag{10}$$

where N is the number of donors and d_i the distance from a donor i to its receptor. Given the interpolation scheme, the matrix can be assembled by correcting the off-diagonal elements, as shown in [22].

2.4 Boundary condition

Boundary conditions for wave generation and active absorption are implemented making use of the IHFOAM toolbox developed by [23]. For all the simulations, the tank bottom is treated as a slip boundary, whereas the no-slip condition is imposed on the floating body surface. Atmospheric condition is used on the top of the wave tank: the velocity boundary condition is set to the so-called *pressureInletOutletVelocity*, a native boundary condition supplied with OpenFOAM®. Such a condition enforces zero derivative in the normal direction to the boundary for all components of the velocity, except for the tangential component of the velocity at points where there is an inflow. In this case a fixed-value boundary condition is applied to the tangential component. The pressure boundary condition is set to *totalPressure*, indicating that for inflow boundary points the static pressure is adjusted according to the velocity. Slip condition is used where the boundary layer development on the wall is safely neglected, since the floating body is sufficiently far away from the walls and it is unaffected by the local flow near the walls.

2.5 Computational model

The semi-submersible OC4 DeepCwind platform is the subject of this study. It is a platform developed as part of the OC4 project, an IEA (International Energy Agency) funded project within the IEA WindTask 30 programme [24]. In the present work, the platform supports the hollow steel tower characterised by the properties indicated in table 1.
Figure 2 shows the platform with the hollow steel tower and a diagram with the degree of freedom of a FOWT, wnereas, figure 3 shows the whole computational domain and the overset mesh details near the body.

3 Results

Figure 4 provides a snapshot of the simulation of the platform floating over a wavy sea. The grid sensitivity analyses is conducted in order to identify the optimal grid resolution.

3.1 Grid sensitivity analysis

Two grids with different resolutions were generated to perform grid convergence tests, composed of a floating-body grid and a background grid. The coarse grid is characterized by 546957 cells, whereas the fine grid has 1341506 cells. Figure 5a shows the surge motion versus time. The results indicate that the two grids can capture the surge motion dynamics in very close agreement. However, as indicated in figure 5b, the coarse mesh provides a different heave motion compared to the fine grid, which is then preferred for the computations discussed in the next section. It is noteworthy that the platform is not at equilibrium in the initial configuration, so that a transient heave oscillation is observed.
Figure 5c provides the sway motion versus time. The platform is uncontrolled and is completely free to move, so that its motion may generate a non-aligned configuration with respect to the waves, which may generate a sway motion. The dynamics of this motion may vary remarkably changing the mesh.

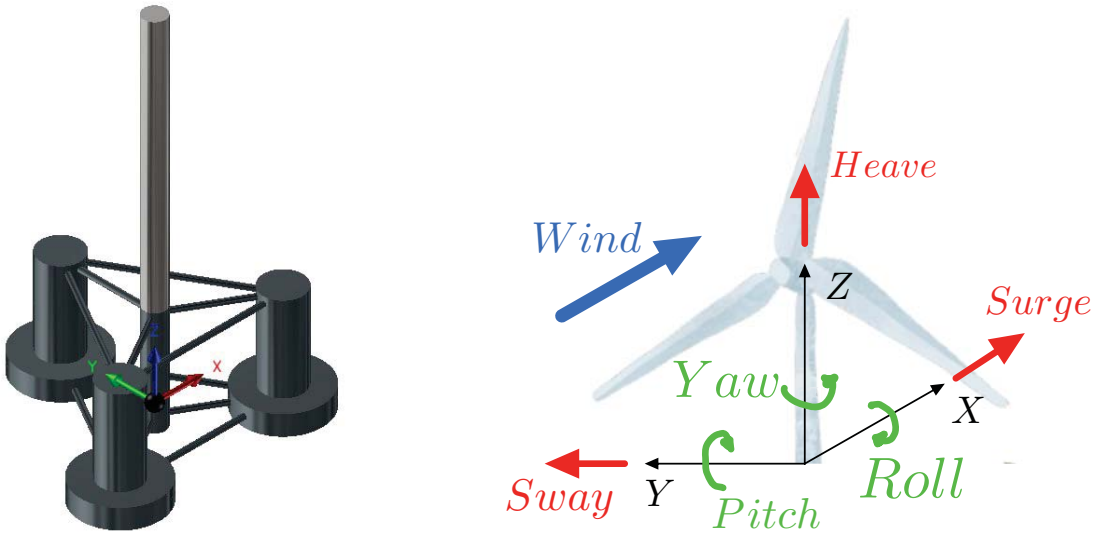

(a) Platform with hollow tower.

(b) Motion types of FOWT.

Figure 2: Platform geometry (left), degrees of freedom (right).

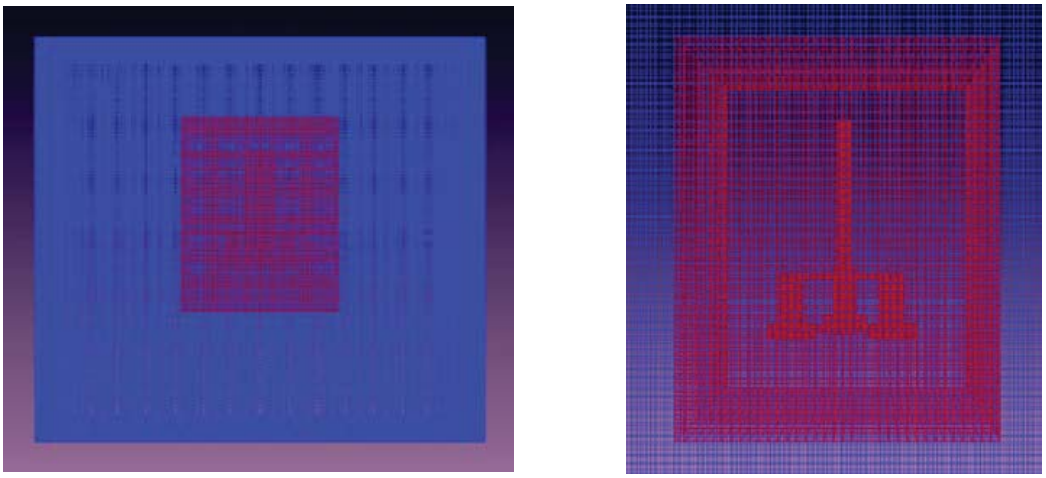

(a) Overall computational domain.

(b) Overset mesh detail.

Figure 3: Computational domain (left) and mesh detail near the moving body (right).

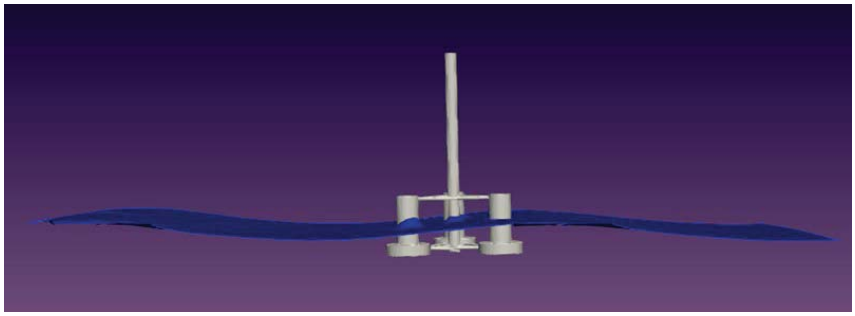

Figure 4: Snapshot of the floating platform simulation.

Concerning the analysis of Euler angles, figure 5d shows that the predicted values of the pitch angle for the coarse and fine meshes are very close. Figure 5e and 5f show that, for the yaw and roll angle, respectively, the coarse mesh provides results clearly different from those provided by the fine mesh. In conclusion, it can be stated that the coarse mesh is unsuitable for carrying out simulations on this case study, as it provides significantly different data compared to the fine mesh. Therefore, it would be suitable to use the fine mesh for the successive numerical study.

3.2 Waves height effects

A comparison is presented between two simulations, which differ only in the value of the wave height. All other parameters are held equal. It is noteworthy that the initial wave interacts with the platform 12.1 seconds after the start of the simulation and has a period of 12.1 seconds. Given that the simulation duration is limited to 60 seconds, only the initial transient dynamics is analysed here. The motion observed before 12.1 seconds is due to the non equilibrium initial configuration of the platform. The first simulation considers a wave height of 5.15 m, whereas the second one presents a wave height of 10.30 m. Figure 6 a-c compare the motion of the centre of mass along the three axes, respectively. It appears that the largest motions are those of surge and heave, in accordance with expectations for a semi-submersible support. The sway motions are found to be approximately three orders of magnitude smaller than those along the other axes. Finally, it can be seen that a wave of twice the height causes surge displacements more than twice as large.
An analysis of the Euler angles along the three axes for the two simulations with different wave heights shows an initial transient followed by an oscillating trend with stabilized amplitude of the oscillations for the pitch and roll angles. The pitch angle, which represents the angle of largest oscillation amplitude, is analysed in detail in figure 6d. The figure illustrates that the qualitative trend observed in the two case studies is similar, although the values are doubled at the extremes in the case of the wave of greater height. Yaw and roll angles show very small oscillations.

3.3 The effect of the tower

In this section we consider two configurations, one with the tower and the other without, all other parameters being the equal. We employ the fine mesh and a wave height of 5.15 m. Firstly, it can be observed that the qualitative trend of the surge and heave motions is very similar. It appears that the presence of the tower shifts the centre of mass of 1.278 m and slightly influence the oscillation dynamics of the system. The sway motion differs between the two cases. This is probably due to the high sensitivity of this motion, which breaks the symmetry of the configuration, as discussed previously. Concerning the Euler angles, the pitch angle time history is barely affected by the presence of the tower. On the other hand, yaw and roll angle variations are very small and follow very different trajectories.

4 Conclusions

In this study, a hydrodynamic analysis of the semi-submersible OC4-DeepCWind platform was conducted using the OpenFOAM software. The OverInterDyMFoam solver was employed to solve the unsteady Reynolds-averaged Navier–Stokes equations governing the two-phase incompressible flow dynamics. This solver is based on the volume-of-fluid approach to capture the surface of separation between seawater and air and employs the PIMPLE algorithm for pressure-velocity coupling. The sixDoFrigidBodyMotion solver is employed to simulate the rigid body dynamics of the system described by six degrees of freedom. The computational domain was discretized by a dynamic overset mesh, which proved to be particularly suitable for tracking the motion of a floating body with a complex geometry. This approach provides accurate solutions by reducing the computational cost through efficient management of the moving meshes, thereby minimising the mesh distortion. The aim of this study is to assess the proposed model through a grid sensitivity study varying the grid resolution. Initially, a grid sensitivity analysis was conducted to ascertain the suitable grid refinement level enabling accurate results with the lowest computational cost. Furthermore, computations were conducted to simulate the interaction of the platform structure (including the tower) with waves of different heights. The results showed that in the presence of double-height waves, the geometry exhibited a larger surge motion in the direction of wave generation. The heave motion exhibited a correct increase with the wave height, thereby confirming the stability of the support. Finally, the impact of incorporating the tower onto the platform was studied. Results indicated that the addition of the tower exerted a slight destabilising influence on the support's dynamic behaviour, specifically on the heave motion due to the elevation of the centre of mass. In conclusion, the model has demonstrated its efficacy as a highly valuable tool for the simulation of wind turbines on floating platform, with

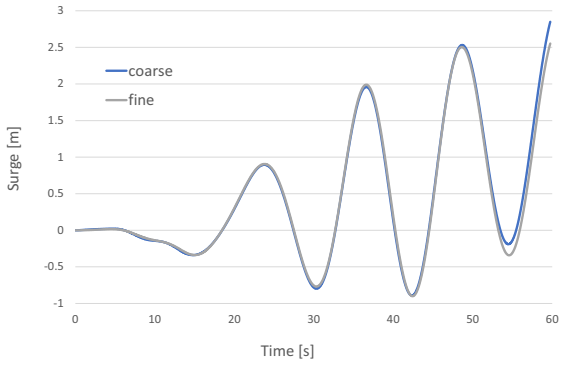

(a) Surge sensitivity to grid resolution.

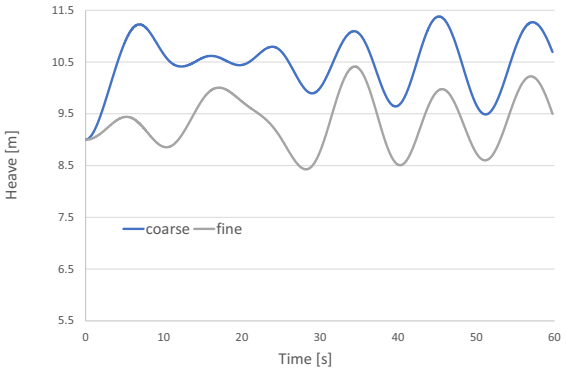

(b) Heave sensitivity to grid resolution.

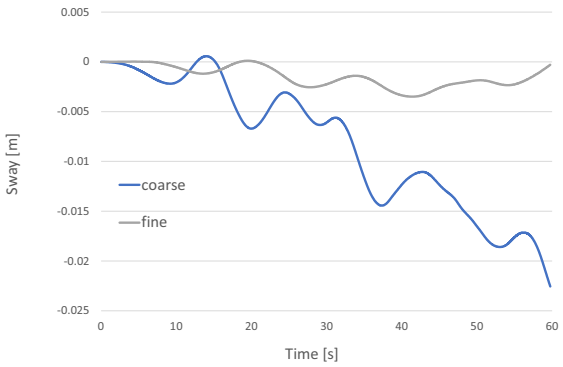

(c) Sway sensitivity to grid resolution.

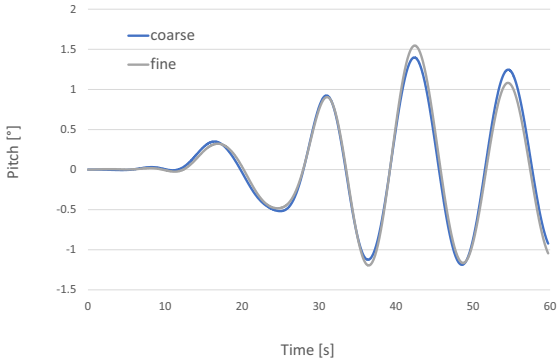

(d) Pitch sensitivity to grid resolution.

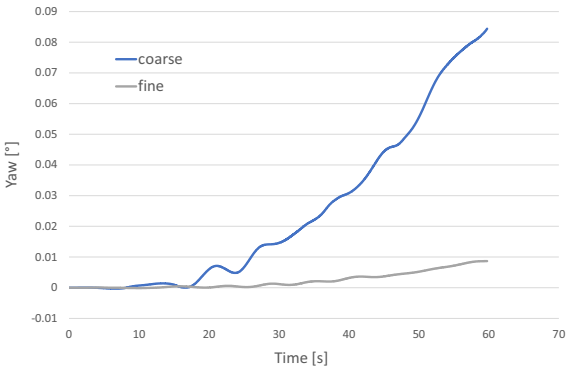

(e) Yaw sensitivity to grid resolution.

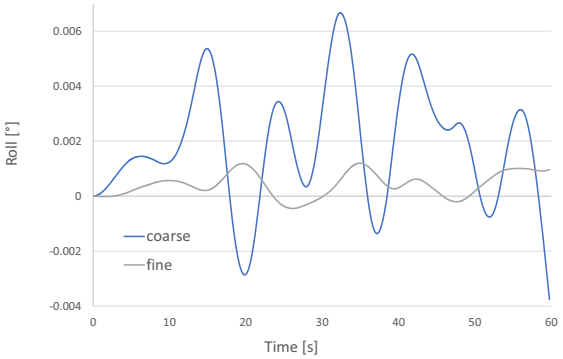

(f) Roll sensitivity to grid resolution.

Figure 5: Sensitivity to grid resolution.

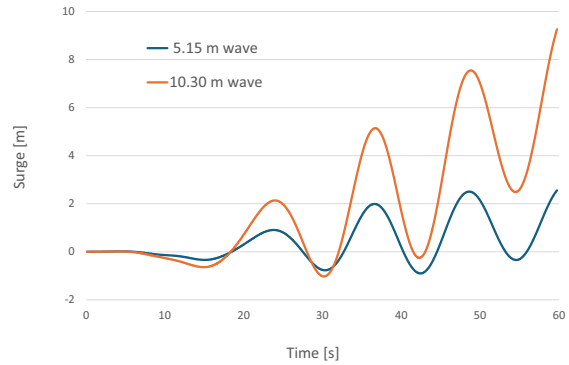

(a) Surge sensitivity to waves' height.

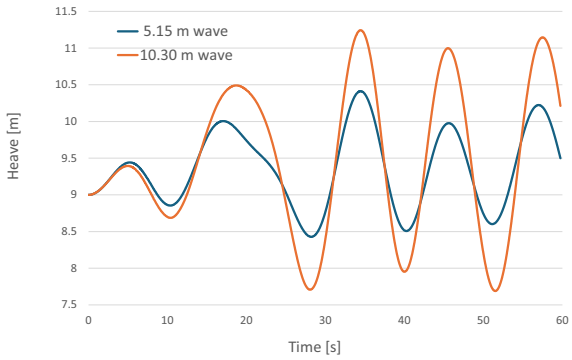

(b) Heave sensitivity to waves' height.

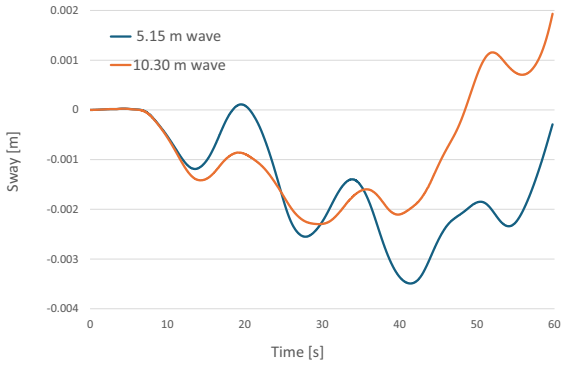

(c) Sway sensitivity to waves' height.

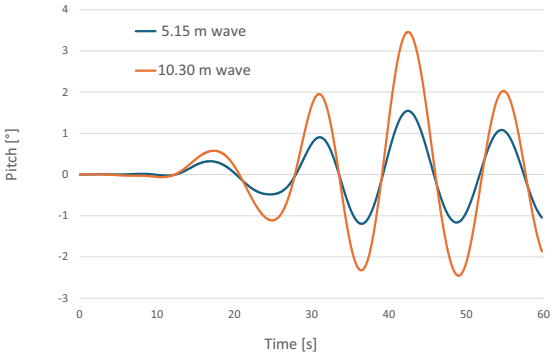

(d) Pitch sensitivity to waves' height.

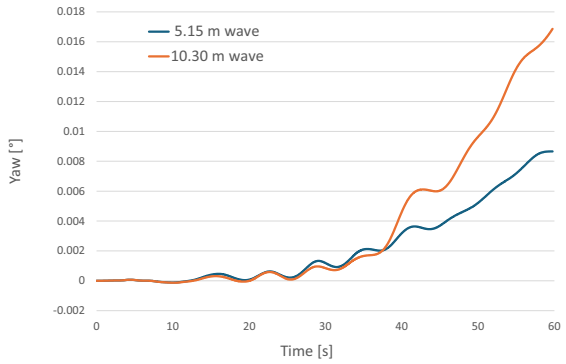

(e) Yaw sensitivity to waves' height.

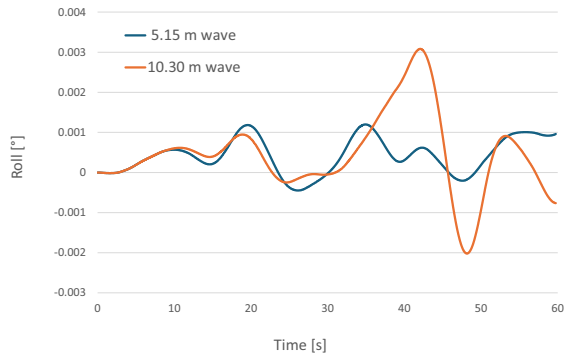

(f) Roll sensitivity to waves' height.

Figure 6: Sensitivity to waves' height.

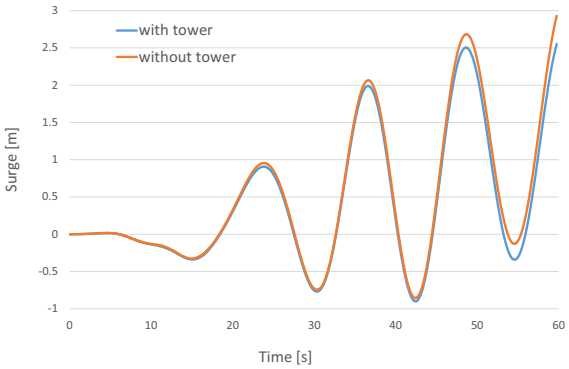

(a) Surge sensitivity to tower presence.

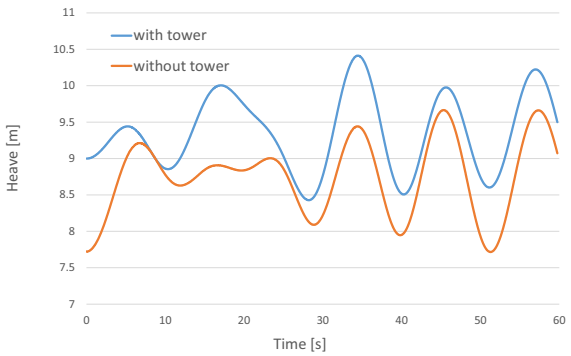

(b) Heave sensitivity to tower presence.

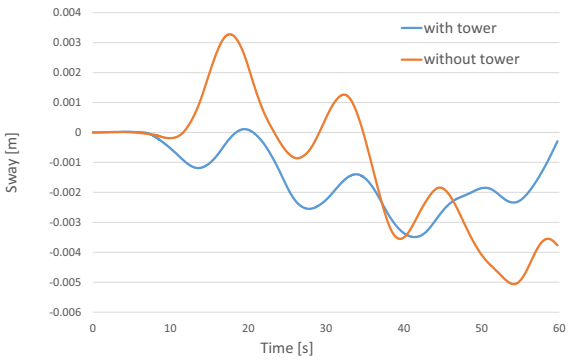

(c) Sway sensitivity to tower presence.

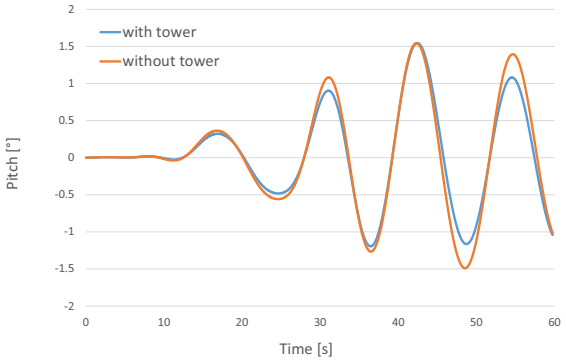

(d) Pitch sensitivity to tower presence.

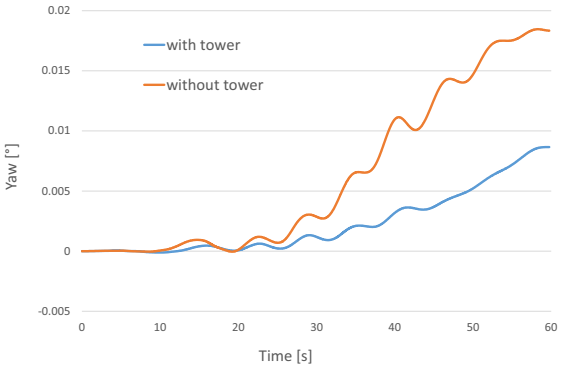

(e) Yaw sensitivity to tower presence.

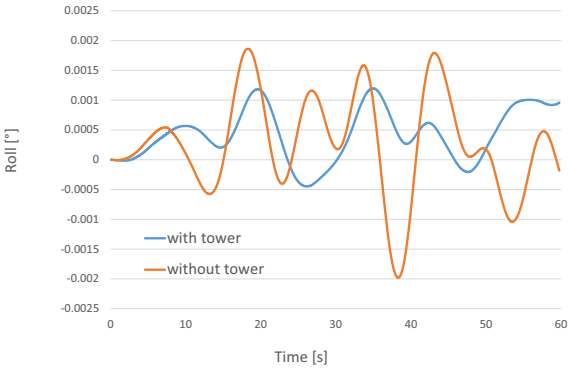

(f) Roll sensitivity to tower presence.

Figure 7: Sensitivity to tower presence.

considerable potential for future developments. These include the extension of the model geometry to encompass the wind turbine itself with the inclusion of a mooring system, with the objective of achieving a complete model that is suitable to accurately simulate the real design case. It is worth noticing that the study considered regular waves (modelled according to the Stokes wave model), which do not fully describe the complexity of real-world wave motion. Moreover, all simulations were performed with a 60-second simulation time, as the aim was to demonstrate the validity of the model. However, during the design phase, longer simulation times should be employed. According to the International Towing Tank Conference guidelines [25], motion data should be collected for at least 10 quasi-stationary cycles under regular wave conditions to ensure the accuracy of the outcomes.

Acknowledgments
Project funded under the National Recovery and Resilience Plan (NRRP), Mission 4 Component 2 Investment 1.3 - Call for tender No. 1561 of 11.10.2022 of Ministero dell'Università e della Ricerca (MUR); funded by the European Union – NextGenerationEU. Project code PE0000021, project title "Network 4 Energy Sustainable Transition – NEST".

References

[1] R. Perveen, N. Kishor, S. R. Mohanty, Off-shore wind farm development: Present status and challenges, Renewable and Sustainable Energy Reviews 29 (2014) 780–792. doi:https://doi.org/10.1016/j.rser.2013.08.108.

[2] M. de Oliveira, R. Puraca, B. Carmo, Blade-resolved numerical simulations of the nrel offshore 5 mw baseline wind turbine in full scale: A study of proper solver configuration and discretization strategies, Energy 254 (2022) 124368. doi:https://doi.org/10.1016/j.energy.2022.124368.

[3] Y. Wang, W. Miao, Q. Ding, C. Li, B. Xiang, Numerical investigations on control strategies of wake deviation for large wind turbines in an offshore wind farm, Ocean Engineering 173 (2019) 794–801. doi:https://doi.org/10.1016/j.oceaneng.2019.01.042.

[4] Y. Wang, W. Miao, Q. Ding, C. Li, B. Xiang, Numerical analysis of a floating offshore wind turbine by coupled aero-hydrodynamic simulation, Journal of Marine Science and Application 18 (2019) 82–92. doi:https://doi.org/10.1007/s11804-019-00084-8.

[5] P. Cheng, Y. Huang, D. Wan, A numerical model for fully coupled aero-hydrodynamic analysis of floating offshore wind turbine, Ocean Engineering 173 (2019) 183–196. doi:https://doi.org/10.1016/j.oceaneng.2018.12.021.

[6] T. T. Tran, D.-H. Kim, The coupled dynamic response computation for a semi-submersible platform of floating offshore wind turbine, Journal of Wind Engineering and Industrial Aerodynamics 147 (2015) 104–119. doi:https://doi.org/10.1016/j.jweia.2015.09.016.

[7] Aiming high rewarding ambition in wind energy, European Wind Energy Association (2015).

[8] Y. Liu, Q. Xiao, A. Incecik, C. Peyrard, D. Wan, Establishing a fully coupled cfd analysis tool for floating offshore wind turbines, Renewable Energy 112 (2017) 280–301. doi:https://doi.org/10.1016/j.renene.2017.04.052.

[9] L. Rapella, D. Faranda, M. Gaetani, P. Drobinski, M. Ginesta, Climate change on extreme winds already affects off-shore wind power availability in europe, Environmental Research Letters 18 (3) (2023) 034040. doi:10.1088/1748-9326/acbdb2.

[10] L. Rapella, D. Faranda, M. Gaetani, P. Drobinski, M. Ginesta, Climate change on extreme winds already affects off-shore wind power availability in europe, Climatic Change 128 (2014) 99–112. doi:https://doi.org/10.1007/s10584-014-1291-0.

[11] F. Vorpahl, H. Schwarze, T. Fischer, M. Seidel, J. Jonkman, Offshore wind turbine environment, loads, simulation, and design, Wiley Interdisciplinary Reviews: Energy and Environment 2 (5) (2013) 548–570.

[12] Y. Zhou, Q. Xiao, Y. Liu, A. Incecik, C. Peyrard, D. Wan, G. Pan, S. Li, Exploring inflow wind condition on floating offshore wind turbine aerodynamic characterisation and platform motion prediction using blade resolved cfd simulation, Renewable Energy 182 (2022) 1060–1079. doi:https://doi.org/10.1016/j.renene.2021.11.010.

[13] A. Corti, C. Chiastra, M. Colombo, M. Garbey, F. Migliavacca, S. Casarin, A fully coupled computational fluid dynamics – agent-based model of atherosclerotic plaque development: Multiscale modeling framework and parameter sensitivity analysis, Computers in Biology and Medicine 118 (2020) 103623. doi:https://doi.org/10.1016/j.compbiomed.2020.103623.

[14] Y. Zhang, B. Kim, A fully coupled computational fluid dynamics method for analysis of semi-submersible floating offshore wind turbines under wind-wave excitation conditions based on oc5 data, Applied Sciences 8 (11) (2018). doi:10.3390/app8112314.

[15] A. Otter, J. Murphy, V. Pakrashi, A. Robertson, C. Desmond, A review of modelling techniques for floating offshore wind turbines, Wind Energy 25 (5) (2022) 831–857. doi:https://doi.org/10.1002/we.2701.

[16] E. Katsidoniotaki, M. Göteman, Numerical modeling of extreme wave interaction with point-absorber using openfoam, Ocean Engineering 245 (2022) 110268. doi:https://doi.org/10.1016/j.oceaneng.2021.110268.

[17] H. Rusche, Computational fluid dynamics of dispersed two-phase flow at high phase fractions, Ph. D. thesis, University of London (2002).

[18] P. Higuera, J. L. Lara, I. J. Losada, Realistic wave generation and active wave absorption for navier–stokes models: Application to openfoam®, Coastal Engineering 71 (2013) 102–118. doi:https://doi.org/10.1016/j.coastaleng.2012.07.002.

[19] N. M. Newmark, A method of computation for structural dynamics, Journal of the Engineering Mechanics Division, 85 (EM3) (3): 67–94 (1959).

[20] W. M. Chan, S. A. Pandya, Advances in distance-based hole cuts on overset grids, in: 22nd AIAA Computational Fluid Dynamics Conference, 2015, p. 3425.

[21] C. T. Druyor Jr, Advances in parallel overset domain asembly (2016).

[22] J. Brunswig, M. Manzke, T. Rung, Explicit and implicit coupling strategies for overset grids, in: Proceedings of the 10th Symposium on Overset Composite Grids and Solution Strategies, NASA AMES Research Center, 2010.

[23] P. Higuera, J. L. Lara, I. J. Losada, Three-dimensional interaction of waves and porous coastal structures using openfoam®. part i: Formulation and validation, Coastal Engineering 83 (2014) 243–258. doi:https://doi.org/10.1016/j.coastaleng.2013.08.010.

[24] A. Robertson, J. Jonkman, M. Masciola, H. Song, A. Goupee, A. Coulling, C. Luan, Definition of the semisubmersible floating system for phase ii of oc4, Tech. rep., National Renewable Energy Lab.(NREL), Golden, CO (United States) (2014).

[25] M. Morabito, J. Park, M. van Rijsbergen, Quality systems group, Tech. rep. (2017).